npj | Materials Degradation

www.nature.com/npjmatdeg

ARTICLE OPEN

Check for updates

A multiparametric study on the dissolution of synthetic brannerite

Hantao Lin[1], Stéphanie Szenknect[1✉], Adel Mesbah[1,2✉], Fabien Baron[3], Daniel Beaufort[3], Yann Batonneau[3], Julien Mercadier[4], Aurélien Eglinger[4], Marion Turuani[5], Anne-Magali Seydoux-Guillaume[5,6], Philippe Goncalves[7], Flavien Choulet[7], Virginie Chapon[8], Maurice Pagel[9] and Nicolas Dacheux[1]

Brannerite, UTi_2O_6 is reported to occur in various uraniferous deposits worldwide. Natural brannerite specimens are found in the amorphous state and are usually considered to be refractory to dissolution due to the formation of TiO_2 passivation layer. In the present work, brannerite was synthesized by wet chemistry route, then characterized prior the development of multiparametric dissolution experiments. The evolution of U and Ti concentrations was followed in 0.1–2 mol/L H_2SO_4 solutions, for temperatures ranging from 25 to 80 °C, in the presence (or not) of 2.8 g/L of dissolved Fe(III). The dissolution of synthetic brannerite was congruent in the whole experimental domain. The formation of Ti-enriched secondary phase at the surface of the brannerite grains was not evidenced. The dissolution rate constants, activation energies and partial orders of the overall dissolution reaction relative to proton activity were determined in the presence (or absence) of Fe(III). The introduction of Fe(III) in sulfuric acid solutions increased the dissolution rate constant by 5 orders of magnitude and induced significant modifications of the apparent activation energy (from 71 ± 4 to 91 ± 6 kJ/mol) and of the partial order relative to proton activity (from 0.42 ± 0.09 to 0.84 ± 0.08). This study suggested that the uncongruency of the brannerite dissolution and the changes usually observed in the rate-controlling step with temperature could be linked to the loss of the crystal structure in natural samples.

npj Materials Degradation (2021)5:30 ; https://doi.org/10.1038/s41529-021-00173-6

INTRODUCTION

The share of nuclear energy has been continuously growing in order to match the high demand of energy with low CO_2 emission. Consequently, there has been a growing need of exploitable natural uranium resources[1]. Due to its abundance, uraninite (UO_{2+x}) is the uranium-bearing phase that is mostly used in the extraction of uranium from ores. The majority of processes used to extract uranium from uraninite involves an acid dissolution step coupled with an oxidation of the tetravalent uranium[2,3]. The economic impact of this step is very important. Its optimization is an absolute prerequisite for the cost-effective exploitation of the uranium deposit. With the exhausting easy exploitable ores, other uranium containing minerals are actually under consideration. Among them, brannerite (UTi_2O_6) is considered to be the third mineral of tetravalent uranium after uraninite and coffinite ($USiO_4$). Consequently, it could be considered as another exploitable source of uranium[4].

Brannerite was found in several places around the world such as Mount Isa (Australia)[5,6], Elliot Lake (Ontario, Canada)[7,8], Crocker Well (Australia)[9], in some different uraniferous deposits in the Witwatersrand area (South Africa)[10] and in the exploited uranium mines of Ranger and Olympic Dam (Australia)[6]. Natural brannerite specimens are found in an amorphous state because of self-radiation (i.e. metamictisation)[11,12]. The recovery of the crystal network requires thermal annealing at 1000 °C. Brannerite mineral is able to incorporate various elements, among which Pb, Ca, Th, Y, and Ce in the U-site and Si, Al, Fe in the Ti-site. It is worth noting that the presence of lead is mainly radiogenic, consequently to the decay chains of U and Th[12,13]. The general formula is close to [U, Ca, Y, Ce, La][Ti, Fe]$_2O_6$[11,14–16]. The crystallized form of brannerite adopts the monoclinic system in the *C*2/*m* space group. The structure of brannerite is characterized by 2D infinite layers formed of TiO_6 octahedra linked to each other by UO_6 octahedra through the *c* axis.

In the literature, brannerite is reported to be difficult to dissolve. Indeed, the recovery of uranium requires the use of aggressive acidic conditions. The major part of research activities was dedicated to dissolution of natural brannerite, and few were dedicated to synthetic samples[11,17–29]. Three parameters have been shown to influence the dissolution rate of natural or synthetic brannerite: temperature, sulfuric acid concentration and redox potential of the leaching solution. From the results reported in the literature, it appeared that the complete recovery of uranium from brannerite could be reached within 1 h in 1 mol/L H_2SO_4 solution at high temperature (i.e ~90 °C) and in the presence of 2.8 g/L (i.e., 0.05 mol/L) of Fe(III)[20].

Based on the results reported, the operating temperature plays a major role in the rate of extraction of uranium and titanium. Using a natural sample from Jakutia deposit (Russia), Gogoleva[25] determined two different activation energies (E_A) depending on the temperature range for the dissolution of brannerite in sulfuric acid solution (0.5 mol/L) containing 0.01 mol/L of Fe(III). Between 15 and 35 °C, the activation energy calculated from the U release in solution was 50.5 kJ/mol, which indicated that the rate-limiting

[1]ICSM, Univ Montpellier, CNRS, CEA, ENSCM, Site de Marcoule, Bagnols-sur-Cèze, France. [2]Univ Lyon, Université Lyon 1, Institut de Recherches sur la Catalyse et l'Environnement de Lyon, IRCELYON, UMR5256, CNRS, Villeurbanne, France. [3]Université de Poitiers, CNRS UMR 7285 IC2MP, HydrASA Bât. B35, Poitiers, France. [4]Université de Lorraine, CNRS, CREGU, GeoRessources Laboratory, B.P. 70239, Vandœuvre-lès-Nancy, France. [5]Univ Lyon, UJM-Saint-Etienne, Saint-Etienne, France. [6]Université de Lyon, UCBL, ENSL, CNRS, LGL-TPE, Villeurbanne, France. [7]Chrono-Environnement, UMR 6249, CNRS-Université de Bourgogne Franche-Comté, Besançon, France. [8]CEA, CNRS, Aix-Marseille Université, UMR 7265 Biologie Végétale et Microbiologie Environnementales, Laboratoire des Interactions Protéine Métal, Saint-Paul-lez-Durance, France. [9]Université de Paris-Saclay, CNRS, GEOPS, ORSAY, France. ✉email: stephanie.szenknect@cea.fr; adel.mesbah@ircelyon.univ-lyon1.fr

Published in partnership with CSCP and USTB

npj nature partner journals

step was a chemical reaction occurring at the solid/solution interface. On the contrary, between 35 and 90 °C, the activation energy decreased down to 30.3 kJ/mol, suggesting the control of the dissolution kinetics by a diffusion step. When studying natural sample from Dieresis deposit (Spain), Gilligan and Nikoloski[20] showed that the activation energy of the brannerite dissolution in sulfuric acid solution doped with Fe(III) also depended on the element considered (U or Ti). Indeed, at low temperatures, the activation energy related to the brannerite dissolution and calculated from U release in solution was 36 kJ/mol, which was significantly lower than that obtained for Ti (i.e., 48 kJ/mol). At higher temperatures, both activation energies were similar and lower (23 kJ/mol), which again suggested the existence of diffusion phenomena controlling the dissolution rate. The transition between these two kinetic regimes occurred at lower temperature for the higher sulfuric acid concentrations. Consequently, the dissolution of brannerite at low temperature, in sulfuric acid media and in the presence of iron could be described by the two following reactions:

$$UTi_2O_6(s) + 2\,FeSO_4^+(aq) \leftrightarrows 2\,TiO_2(s) + UO_2(SO_4)_2^{2-}(aq) + 2\,Fe^{2+}(aq) \quad (1)$$

With $E_A(U) = 36$ kJ/ mol

$$TiO_2(s) + 2\,H^+(aq) + SO_4^{2-}(aq) \leftrightarrows TiOSO_4(aq) + H_2O \quad (2)$$

With $E_A(Ti) = 48$ kJ/mol

The first reaction corresponds to the oxidative dissolution of brannerite, U(IV) being oxidized by Fe(III) and solubilized as U(VI) species at the solid/solution interface. This reaction leads to the precipitation of TiO_2 (anatase) as a secondary phase. The second reaction, which is the dissolution of highly refractory TiO_2 layer at the sample surface is controlled by surface reaction involving protons. Consequently, this reaction shows a greater dependence on the concentration of sulfuric acid. At high temperature, the rapid formation of the TiO_2 layer through reaction (1) leads to the passivation of the brannerite surface. The diffusion of reactive species through this layer becomes the rate-limiting step.

Besides the effect of temperature, increasing the sulfuric acid concentration has a positive impact on the dissolution rate of uranium, and has even a stronger effect on the dissolution rate of titanium. It is worth noting that Gogoleva[25] reported a partial order of U dissolution reaction related to the total sulfuric acid concentration of 0.69 at 70 °C in the presence of Fe(III) ions (with a concentration of 0.01 mol/L). At low sulfuric acid concentrations (i.e., from 0.1 to 0.25 mol/L) and especially at elevated temperature (96 °C), Gilligan et al.[20], noticed that the concentration of titanium in the solution decreased markedly after an initial release. Titanium was found to precipitate as anatase (TiO_2) through the hydrolysis of $TiO^+_{(aq)}$, which is thermodynamically favored at low pH. This observation was consistent with the results obtained earlier by Costine et al.[29], who identified a strong correlation between the amount of unleached uranium and the presence of anatase in brannerite dissolution residues.

Costine et al.[29] used natural brannerite samples from the Dieresis deposit to investigate the effect of redox potential and the particle size on brannerite dissolution. The effect of redox potential was investigated by varying the Fe(II)/Fe(III) ratio at a fixed total iron concentration. At 25 and 45 °C, they showed a weak dependence of the uranium extraction on the redox potential while at 65 °C, the extent of uranium extraction reached a maximum at Eh = 460 mV vs. Ag/AgCl. Increasing or decreasing the redox potential led to lower uranium extraction rate. An optimized Fe(III) concentration of 0.01 mol/L was also determined by Gogoleva[25] in 0.5 mol/L H_2SO_4 solution at 70 °C. Below this value, the partial order of the overall U dissolution reaction related to the total Fe(III) concentration was found to be 0.5. Increasing the concentration above this value led to the decrease of U dissolution rate.

Considered as an issue for uranium extraction from ores, the chemical durability of brannerite is also viewed as a major advantage for the immobilization of actinides in the field of radioactive waste management. Thus, brannerite was also considered as a potential waste form and entered the composition of several Synroc families[30–32] or glass-ceramics[33]. Several studies[28,32,34] investigated the leaching of brannerite-bearing waste forms under conditions representative for waste disposal. The release of uranium from synthetic brannerite was modeled as a function of pH and carbonate concentration in oxygenated water by analogy with UO_2. The mechanism consisted in two reaction steps: oxidation of U(IV) by dissolved O_2 at the surface of brannerite, then subsequent detachment of U(VI) species in the solution. Multiparametric rate laws have been established in order to quantify the promoting effect of surface coordination with protons or carbonate species. The partial order of the overall reaction related to proton activity was found between 0.4 and 0.45 for temperature ranging between 50 and 90 °C. Incongruent dissolution was observed, aqueous Ti concentration being limited by the solubility of Ti oxides or hydroxides over the whole range of conditions studied. TiO_2-rich surface alteration products were evidenced at the solid/solution interface. However, under these conditions, the existence of saturation phenomena did not influence strongly the rate of release of uranium.

The majority of the reported studies were dedicated to uranium extraction from natural samples in sulfuric acid conditions and in the presence of Fe(III) used as an efficient oxidant of U(IV). Although these studies were of great importance to optimize U extraction from ores and strongly improved our understanding of the dissolution mechanism, dissolution rate laws were rarely established and when it was done, the kinetic parameters obtained appeared to be deposit-specific. In parallel, the kinetics of dissolution of synthetic brannerite considered as a potential nuclear waste form was studied under much less aggressive conditions. In this field, rate laws were derived that allowed to predict the behavior of brannerite-bearing waste forms over a wide range of repository conditions. In this paper, we decided to combine both approaches and to perform a multiparametric study of brannerite dissolution using pure synthetic sample. We investigated the impact of H_2SO_4 concentration and temperature with or without Fe(III) added to the solution. The aim was to determine kinetic parameters and rate laws characteristic of the brannerite crystal structure, which is hardly achievable with natural samples. The metamictisation, the presence of associated gangue minerals, of oxidized uranium and of substitutions that modify the structure of brannerite all have potential competing or synergetic impacts on the uranium extraction rate that can be further quantified against the results obtained in this work with pure synthetic brannerite.

RESULTS AND DISCUSSION

Evolution of the normalized weight loss during brannerite dissolution: general behavior

The shape of the brannerite dissolution curves was similar whatever the experimental conditions. As representative examples, the evolutions of the relative mass loss and of the normalized weight loss during the dissolution of synthetic brannerite in 2 mol/L H_2SO_4 solution in the presence of Fe(III) at 25 and 80 °C are presented in Fig. 1a, b, respectively. At room temperature (Fig. 1a), the presence of an initial dissolution pulse was clearly evidenced. A similar phenomenon was observed during the dissolution of UO_2 in diluted nitric acid solutions[35]. By analogy, this initial fast release of uranium and titanium was attributed to the presence of a small fraction of more reactive powder. The higher reactivity of this

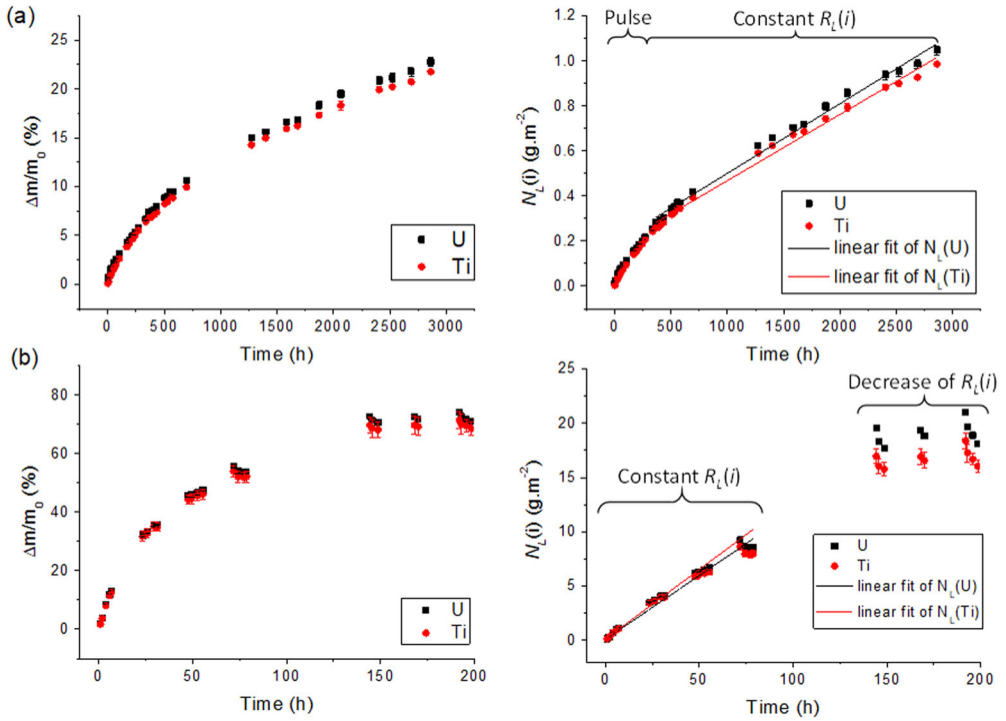

Fig. 1 Released U and Ti during the dissolution of brannerite in 2 mol/L H_2SO_4 with 2.8 g/L of Fe(III). Evolution of the relative mass losses $\Delta m_i/m_0$ (%) and of the normalized weight losses $N_L(i)$ (g/m^2) obtained during the dissolution of synthetic brannerite samples in 2 mol/L H_2SO_4 solution with 2.8 g/L of Fe(III) at 25 °C (**a**) and at 80 °C (**b**).

fraction of brannerite material could be caused by a lower grain size, and/or by an oxidized layer. Grinding of the sample favors the surface oxidation of U(IV) materials and sieving generally does not allow to avoid the presence of a dissolution pulse. This initial release always corresponded to a relative weight loss in the range between 0.1 and 1%. As this part of the dissolution curve appeared not reproducible, it was not considered anymore to determine the normalized dissolution rate. Then, the normalized weight loss increased linearly until a relative mass loss of ~50% was obtained. During this steady step, the specific surface area of the sample could be considered as constant and the normalized dissolution rate was determined. Afterwards (Fig. 1b), a decrease of the normalized dissolution rate was finally observed especially when using very aggressive conditions. In that case, high dissolution progress was obtained within short time scale and this third step was reached. As Fe(III) ions were introduced in solution in large excess, the decrease of the dissolution rate for $\Delta m/m_0 \geq 50\%$ could not be caused by a significant decrease of Fe(III) concentration. This phenomenon was rather attributed to the significant decrease of the reactive surface area of the sample, which is not considered in the calculation of the normalized weight loss (Eq. 4). As, the powdered sample of brannerite was not sieved, a significant fraction of the sample could have a coarse grain size with a low reactivity[25]. The decrease of the normalized weight loss could be also attributed to passivation caused by the surface precipitation of refractory TiO_2. Nevertheless, the formation of TiO_2 as a secondary phase appeared in contradiction with the congruent character of the dissolution. Additionally, it was possible to collect and to analyze by PXRD insoluble residues at the end of some of the leaching experiments. Examples of the collected PXRD patterns are presented in Fig. 2 and are compared with the pattern of the as-synthesized brannerite. The apparition of a very slight diffraction peak around 28° in 2θ corresponding to the potential presence of a very low amount of UO_2. Besides, the presence of neoformed phases such as TiO_2 was not evidenced. The variation of the intensity between the different patterns were

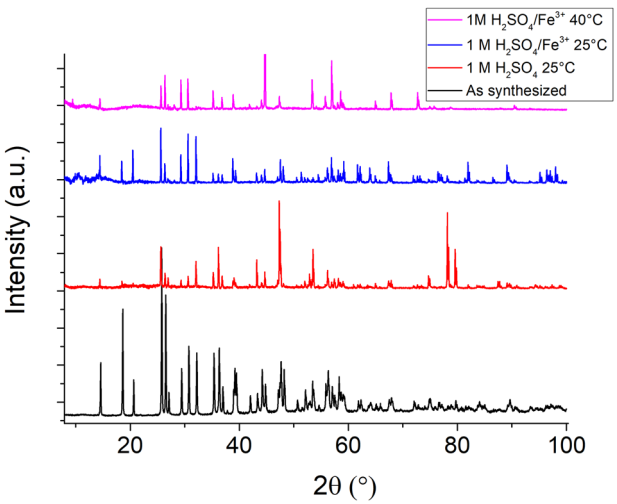

Fig. 2 Powder X-Ray Diffraction (PXRD) patterns of dissolved brannerite samples. PXRD patterns corresponding to the brannerite samples obtained after leaching experiments labeled 2, 5, and 11 (see Table 3).

attributed to the presence of preferred orientation of the remaining large brannerite grains.

The normalized dissolution rates and the congruence ratios determined in the second step (i.e., during the linear evolution of $N_L(i)$) are gathered in the Table 1 for all the conditions investigated. From the results reported in this table, it was found that addition of 2.8 g/L of Fe(III) led to the strong increase of the dissolution rate of brannerite for all the experimental conditions examined. However, the influences of temperature and acid concentration were different in the presence (or not) of Fe(III).

Table 1. Normalized dissolution rates $R_L(U)$ and $R_L(Ti)$ obtained during the dissolution of synthetic brannerite samples in various conditions (with and without Fe(III)). Associated congruence ratios, $R = R_L\ (U)/R_L(Ti)$.

	$[H_2SO_4]$ (mol/L)	$R_L(U)$ (g/(m^2.h))	$R_L(Ti)$ (g/(m^2.h))	$R = R_L(U)/R_L(Ti)$
25 °C	0.1	$(4.72 \pm 0.05) \times 10^{-6}$	$(3.62 \pm 0.07) \times 10^{-6}$	1.30 ± 0.01
	1	$(5.49 \pm 0.08) \times 10^{-6}$	$(5.27 \pm 0.04) \times 10^{-6}$	1.04 ± 0.01
	2	$(7.57 \pm 0.07) \times 10^{-6}$	$(7.40 \pm 0.04) \times 10^{-6}$	1.02 ± 0.01
40 °C	0.1	$(1.08 \pm 0.04) \times 10^{-5}$	$(7.2 \pm 0.3) \times 10^{-6}$	1.49 ± 0.02
	1	$(1.91 \pm 0.05) \times 10^{-5}$	$(1.86 \pm 0.06) \times 10^{-5}$	1.03 ± 0.01
	2	$(2.65 \pm 0.04) \times 10^{-5}$	$(2.58 \pm 0.04) \times 10^{-5}$	1.03 ± 0.01
60 °C	0.1	$(3.48 \pm 0.06) \times 10^{-5}$	$(3.68 \pm 0.06) \times 10^{-5}$	0.95 ± 0.01
	1	$(8.93 \pm 0.06) \times 10^{-5}$	$(8.72 \pm 0.06) \times 10^{-5}$	1.02 ± 0.01
	2	$(1.41 \pm 0.01) \times 10^{-4}$	$(1.31 \pm 0.02) \times 10^{-4}$	1.08 ± 0.01
80 °C	0.1	$(1.70 \pm 0.03) \times 10^{-4}$	$(1.16 \pm 0.02) \times 10^{-4}$	1.46 ± 0.01
	1	$(7.04 \pm 0.07) \times 10^{-4}$	$(6.80 \pm 0.06) \times 10^{-4}$	1.03 ± 0.01
	2	$(1.06 \pm 0.01) \times 10^{-3}$	$(1.08 \pm 0.01) \times 10^{-3}$	1.29 ± 0.01
With 2.8 g/L of Fe (III)				
25 °C	0.1	$(3.3 \pm 0.1) \times 10^{-5}$	$(2.4 \pm 0.1) \times 10^{-5}$	1.37 ± 0.03
	1	$(3.07 \pm 0.09) \times 10^{-4}$	$(3.01 \pm 0.08) \times 10^{-4}$	1.02 ± 0.01
	2	$(3.09 \pm 0.06) \times 10^{-4}$	$(2.94 \pm 0.06) \times 10^{-4}$	1.05 ± 0.01
40 °C	0.1	$(1.04 \pm 0.04) \times 10^{-4}$	$(7.7 \pm 0.3) \times 10^{-5}$	1.36 ± 0.01
	1	$(1.00 \pm 0.03) \times 10^{-3}$	$(9.2 \pm 0.4) \times 10^{-4}$	1.08 ± 0.01
	2	$(8.4 \pm 0.2) \times 10^{-4}$	$(7.2 \pm 0.3) \times 10^{-4}$	1.17 ± 0.01
60 °C	0.1	$(4.4 \pm 0.1) \times 10^{-4}$	$(4.2 \pm 0.1) \times 10^{-4}$	1.04 ± 0.01
	1	$(9.7 \pm 0.2) \times 10^{-3}$	$(8.7 \pm 0.2) \times 10^{-3}$	1.11 ± 0.01
	2	$(1.40 \pm 0.03) \times 10^{-2}$	$(1.33 \pm 0.03) \times 10^{-2}$	1.05 ± 0.01
80 °C	0.1	$(2.9 \pm 0.1) \times 10^{-3}$	$(2.6 \pm 0.1) \times 10^{-3}$	1.11 ± 0.01
	1	$(1.02 \pm 0.01) \times 10^{-1}$	$(9.1 \pm 0.1) \times 10^{-2}$	1.13 ± 0.01
	2	$(1.20 \pm 0.03) \times 10^{-1}$	$(1.11 \pm 0.03) \times 10^{-1}$	1.08 ± 0.01

In order to evidence the impact of temperature on the dissolution rate in both cases, two sets of dissolution experiments were conducted with various acid concentrations at 25, 40, 60, and 80 °C. The evolution of the normalized weight losses $N_L(U)$ and $N_L(Ti)$ obtained in 2 mol/L H_2SO_4 solution without and with Fe(III) are plotted in Figs. 3 and 4, respectively. The results showed that the normalized dissolution rate was strongly dependent on temperature either in the presence or absence of Fe(III). In addition, for the four temperatures studied, the normalized weight losses $N_L(U)$ and $N_L(Ti)$ were nearly the same, showing that the dissolution was congruent under the experimental conditions investigated.

The evolution of the normalized weight loss of brannerite calculated from the releases of uranium and titanium obtained at room temperature in various sulfuric acid concentrations and without Fe(III) is presented in Fig. 5. Under these conditions, the impact of an increase of the sulfuric acid concentration was found to be low. Indeed, when the acid concentration increased from 0.1 to 2 mol/L, the normalized dissolution rate $R_L(U)$ increased only by a factor of 1.6, i.e. from $(4.72 \pm 0.05) \times 10^{-6}$ g/(m^2 h) to $(7.57 \pm 0.07) \times 10^{-6}$ g/(m^2 h) (Table 1). Moreover, the examination of the $R_L(U)$ values reported in Table 1 showed that the impact of the acid concentration was enhanced with temperature. Increasing the sulfuric acid concentration from 0.1 to 2 mol/L led to the increase of the $R_L(U)$ values by a factor of 6.2 at 80 °C. The evolution of the normalized weight loss of brannerite calculated from the uranium and titanium releases obtained at room temperature in various sulfuric acid concentrations and in presence of Fe(III) is shown in Fig. 6. The impact of the sulfuric acid concentration was stronger when introducing Fe(III) in the solution. For instance, at 25 °C, the normalized dissolution rate $R_L(U)$ increased by a factor of 9.4, from $(3.3 \pm 0.1) \times 10^{-5}$ g/(m^2 h) to $(3.09 \pm 0.06) \times 10^{-4}$ g/(m^2 h), when the acid concentration raised from 0.1 to 2 mol/L (Table 1). Once again, the impact of the acid concentration was even more pronounced at high temperature since an increase of $R_L(U)$ by a factor of 41 was observed at 80 °C when the acid concentration increased from 0.1 to 2 mol/L (i.e., from $(2.9 \pm 0.1) \times 10^{-3}$ to $(1.20 \pm 0.03) \times 10^{-1}$g/(m^2 h)). These results indicated that, either in absence or in the presence of Fe(III) in sulfuric acid solutions, the impact of the temperature and of the acidity were not independent. It is also noteworthy that in both cases, the dissolution remained congruent even for low H_2SO_4 concentrations.

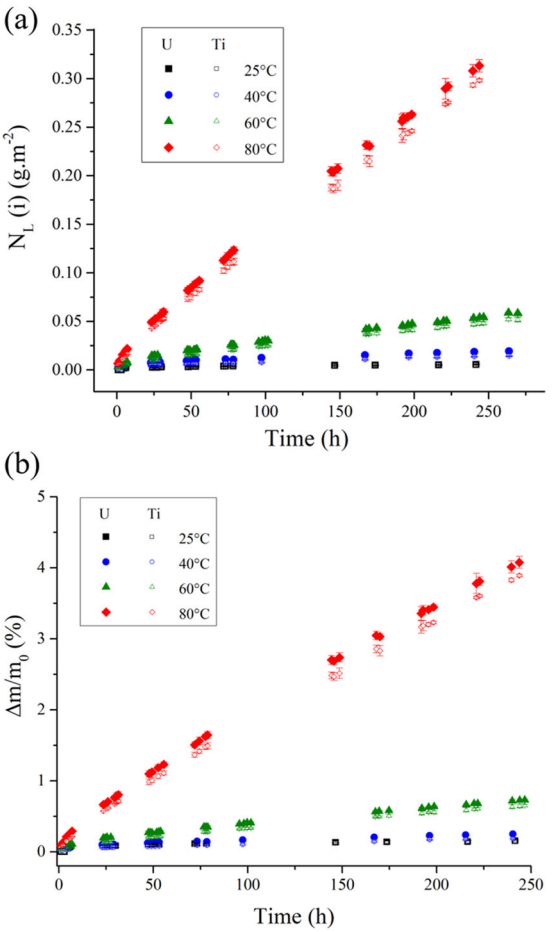

Fig. 3 Dissolution of brannerite in 2 mol/L H_2SO_4. Evolution of the normalized weight losses $N_L(i)$ (g/m^2) (**a**) and of the relative mass losses $\Delta m_i/m_0$ (%) (**b**) obtained during the dissolution of synthetic brannerite sample in 2 mol/L H_2SO_4 solution for various temperatures.

Establishment of multiparametric rate laws

The variations of $R_L(U)$ versus T and $\log(H_3O^+)$ are plotted in Fig. 7 when adding or not Fe(III) in the dissolution media. This figure highlights the strong impact of the addition of Fe(III) to the sulfuric acid solution on the kinetics of dissolution in all the experimental domain. The two sets of data were used independently to determine the three parameters of the multiparametric expression (Eq. 8). The fitted activation energy, E_A, the normalized dissolution rate constant, k, and the partial order of the reaction relative to the proton activity, n, are summarized in Table 2. In order to show the agreement between experiments and modeling, the data

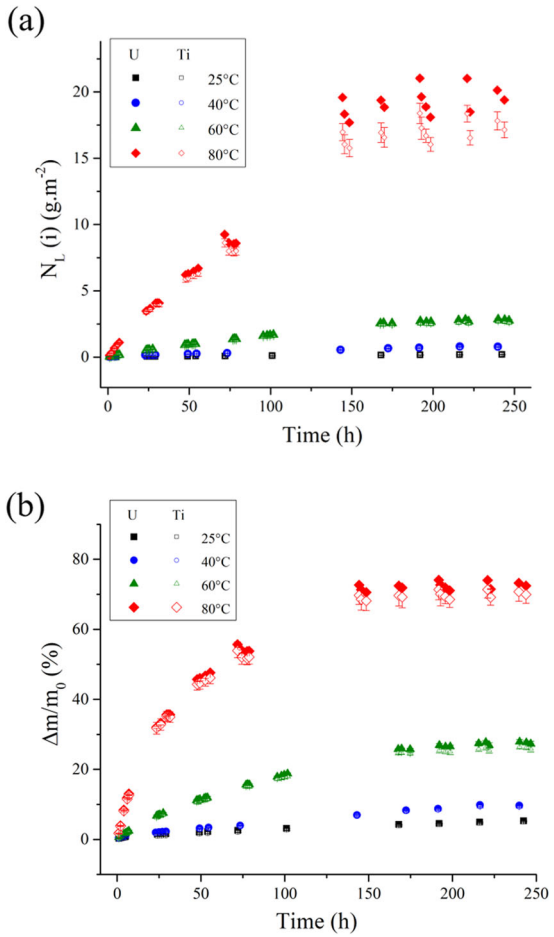

Fig. 4 Dissolution of brannerite in 2 mol/L H_2SO_4 with 2.8 g/L of Fe (III). Evolution of the normalized weight losses N_L(i) (g/m^2) (**a**) and of the relative mass losses $\Delta m/m_0$ (%) (**b**) obtained during the dissolution of synthetic brannerite samples in 2 mol/L H_2SO_4 solution containing 2.8 g/L of Fe(III) for various temperatures.

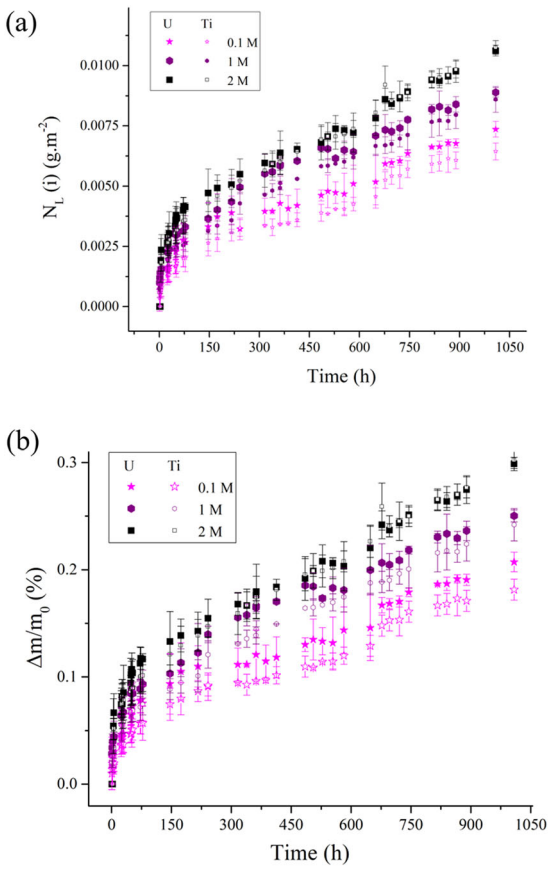

Fig. 5 Dissolution of brannerite in H_2SO_4 solutions at 25 °C. Evolution of the normalized weight losses N_L(i) (g/m^2) (**a**) and of the relative mass losses $\Delta m_i/m_0$ (%) (**b**) obtained during the dissolution of synthetic brannerite samples in various H_2SO_4 solutions at 25 °C.

simulated on the whole experimental domain using Eq. (8) and the fitted parameters are plotted as colored maps in Fig. 7. Additionally, Supplementary Fig. S1 of the supporting data shows the comparison of simulated and experimental data.

From the analysis of the fitted parameters (Table 2), it appears that the introduction of Fe(III) in the system strongly increased the dissolution rate constant, *k*, by 5 orders of magnitude. It is now acknowledged that in the presence of oxidative species in solution regarding to U(IV), the dissolution of U(IV)-bearing phases must be considered as a corrosion reaction, in which the oxidant is consumed to convert the insoluble U(IV) species to the much more soluble U(VI) species (as $UO_2^{2+}{}_{(aq)}$) in the solution. The rate of this reaction should depend on redox conditions, as already demonstrated for uraninite[36–42].

The thermodynamic driving force for such a corrosion process is the difference existing between the redox potential of the solution and the potential associated to the U(IV)/U(VI) couple at the brannerite/solution interface. Increasing the redox potential of the dissolution medium leads to an increase of this driving force. For this reason, oxidants like Fe(III) are added to the leaching solution to improve the kinetics of dissolution of refractory U(IV) phases compared to solutions in equilibrium with atmosphere. However, Costine et al.[29] showed a complex dependence of the dissolution rate of brannerite with redox potential of the solution.

In the absence of Fe(III) and operating in less aggressive conditions, Thomas and Zhang[34] reported that uranium release was dependent on the activity of dissolved dioxygen. By analogy with UO_2, they assumed that the brannerite dissolution mechanism consisted in two successive reactions. The first was the oxidation of U(IV) to U(VI) by $O_{2\ (aq)}$ at the solid/solution interface. The second reaction involved the adsorption of protons and/or surface complexation of uranium (VI) sites at the surface, followed by the detachment of uranium (VI) based species. Under the conditions investigated by Thomas and Zhang[34], the first reaction was the rate-limiting step, especially when carbonate ions were added to the solution. Carbonates are considered as ligands, which promote the detachment of U(VI) species from the brannerite surface. The comparison of complexation constants of $UO_2^{2+}{}_{(aq)}$ with $CO_3^{2-}{}_{(aq)}$ or $SO_4^{2-}{}_{(aq)}$ gives insights for the magnitude of the ligand-promoted detachment phenomenon. Guillaumont et al.[43] reported that log $K°$(298 K) of the reaction $UO_2^{2+}{}_{(aq)} + 2\ L^{2-}{}_{(aq)} \leftrightarrows UO_2(L)_2^{2-}{}_{(aq)}$ equals 16.61 ± 0.09 and 3.02 ± 0.38 for $L^{2-} = CO_3^{2-}{}_{(aq)}$ and $SO_4^{2-}{}_{(aq)}$, respectively. Assuming that the tendency to form more soluble surface complexes increases with the tendency to form aqueous complexes, sulfate ions are less efficient than carbonates in increasing the detachment step. Similar analysis was made by Gilligan et al.[24] to explain the lower efficiency of the ferric chloride/hydrochloric acid system than the acidic ferric sulfate media to extract uranium from brannerite. It could be concluded that the oxidation of U(IV) by O_2(aq) at the surface sites was the rate-limiting step in our study in the absence of Fe(III). Adding Fe(III) increased the redox potential of the leaching solution and might increase the rate of the first oxidation step.

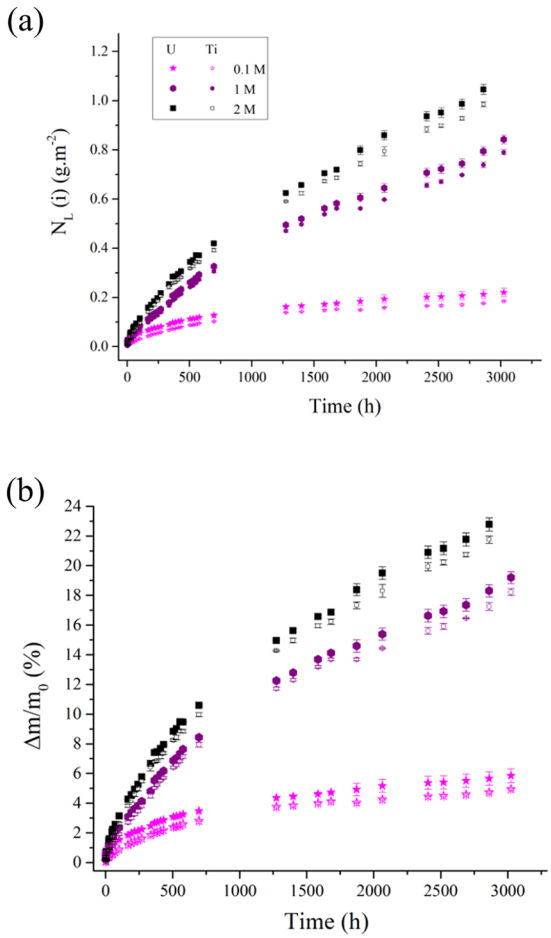

Fig. 6 Dissolution of brannerite in H_2SO_4 solutions with 2.8 g/L of Fe(III) at 25 °C. Evolution of the normalized weight losses N_L(i) (g/m^2) (**a**) and of the relative mass losses $\Delta m_i/m_0$ (%) (**b**) obtained during the dissolution of synthetic brannerite samples in various H_2SO_4 solutions containing 2.8 g/L of Fe(III) at 25 °C.

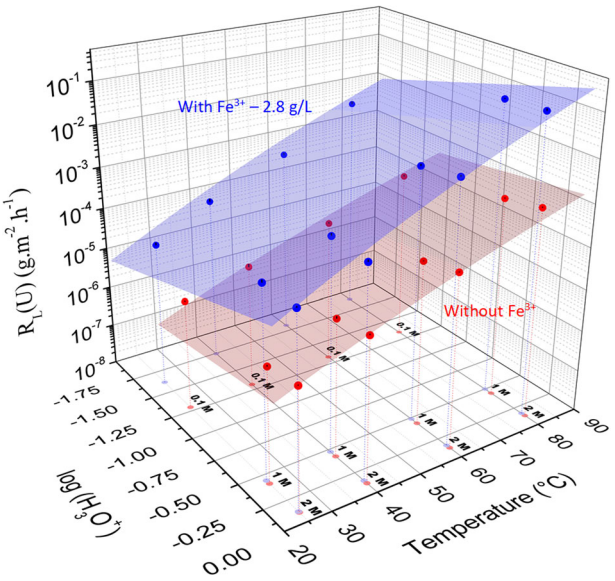

Fig. 7 Experimental and simulated dissolution rates of brannerite. Simulated maps obtained by fitting the multiparametric expression of the normalized dissolution rate of synthetic brannerite samples based on the data obtained without (red dots) or with (blue dots) Fe(III) in sulfuric acid solutions.

Table 2. Values of log k, E_A and n fitted from the R_L(U) values obtained in the presence or in the absence of Fe(III) with various acid concentrations and temperatures.

	Without Fe(III)	With Fe(III) (2.8 g/L)
log k (g/(m^2 h))	7.2 ± 0.7	12.4 ± 0.9
E_A (kJ/mol)	71 ± 4	91 ± 6
n	0.42 ± 0.09	0.84 ± 0.08

The magnitude of the E_A is also an important indicator of the nature of the rate-limiting reaction[44]. The obtained values of E_A were 71 ± 4 and 91 ± 6 kJ/mol in the absence and in the presence of Fe(III), respectively for the whole temperature range investigated (i.e. 25–80 °C). Such high values were not compatible with diffusion-controlled mechanism, which are usually relatively independent of temperature (with $E_A < 20$–25 kJ/mol). Such E_A values were also significantly higher than those reported in the literature[9,20,25] for natural brannerite samples in the presence of Fe (III), but in agreement with the values obtained by Zhang et al.[32] for synthetic brannerite in the absence of Fe(III) (i.e., 70 kJ/mol). E_A value obtained in this work without Fe(III) added to the dissolution media was found to be in the upper range, but still compatible with surface reactions controlling phenomena at the solid/liquid interface (typically between 40 and 80 kJ/mol). This strong discrepancy could be related to the metamictization of brannerite natural samples, which destroys the crystal structure. The complete loss of the crystalline structure could influence the kinetics of brannerite dissolution, or change the nature of the rate-limiting step. Due to radiation damage, U and Ti could be located in independent entities at the atomic scale. Thus, only U-rich entities might be reactive, their specific dissolution leaving behind a surface layer of Ti-rich entities acting as a diffusion barrier for the species in solution responsible for U(IV) oxidation.

The partial order of reaction related to the protons activity obtained in this work ($n = 0.42 \pm 0.09$) in the absence of Fe(III) was in agreement with the value reported by Thomas and Zhang[34] when working on synthetic brannerite in less aggressive conditions (i.e. between 0.4 and 0.45 in a temperature range of 50–90 °C). Gogoleva[25] also reported a partial order of U dissolution reaction related to the total sulfuric acid concentration of 0.69 at 70 °C in ferric media (Fe(III) = 0.01 mol/L), whereas Gilligan et al[24]. reported 0.43 and 0.57 for U and Ti, respectively in 0.1 to 2 mol/L H_2SO_4 solutions at 52 °C. These values were not directly comparable to the value obtained in this work ($n = 0.84 \pm 0.08$). Unlike the formers, the latter was valid in the whole temperature range investigated and was related to the (H_3O^+) activity in the leaching solution (not to the acid concentration). This n value indicates that the adsorption of protons occurs onto the surface of the brannerite, then protonated U and/or Ti surface species are detached from the brannerite lattice.

As conclusion, multiparametric dissolution experiments were conducted on pure synthetic brannerite samples. Normalized dissolution rates were evaluated under various temperatures (from 25 to 80 °C) and sulfuric acid concentrations (from 0.1 to 2 mol/L), either in the absence or in the presence of 2.8 g/L of Fe (III) in the dissolution media. Multiparametric dissolution rate laws were established with and without Fe(III) and the modeled parameters were found to be valid in the whole temperature and acidity ranges. As expected, the introduction of Fe(III) in the solution strongly increased the normalized dissolution rate of the sample and modified the activation energy and the partial order of the overall dissolution reaction related to protons activity. Contrary to what has been reported in the literature for natural

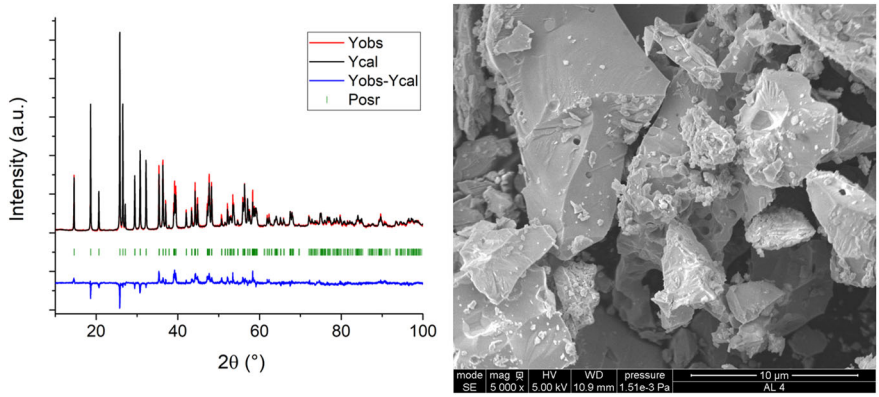

Fig. 8 PXRD and SEM images of as-prepared brannerite sample. Observed, calculated, and the difference patterns after the Rietveld refinement of the crystal structure of brannerite (left panel), SEM image of the brannerite grains used for the dissolution experiments (right panel).

brannerite samples, the dissolution was found to be congruent in the whole experimental domain examined. Both U and Ti releases in solution were controlled by chemical reactions involving the oxidant (either O_2(aq) or Fe(III)) and protons at the solid/solution interface. The role of sulfate ions was not explicitly studied, but they are expected to kinetically favor the step of detachment of U(VI) species from the surface of the solid. The two-steps mechanism described from experiments performed with natural samples, which involved the dissolution in acidic media of a neoformed TiO_2 layer at the surface of brannerite was not valid for synthetic samples. This strong discrepancy could be related to the metamictization of brannerite natural samples, which destroy the crystal structure. Due to radiation damage, U and Ti could be located in independent entities at the atomic scale. Thus, only U-rich entities might be reactive, their specific dissolution leaving behind a surface layer of Ti-rich entities acting as a diffusion barrier for the species in solution responsible for U(IV) oxidation. The analysis of the alteration layer of natural brannerite grains at the atomic scale could bring key information to support this assumption.

METHODS

Synthesis

NH_4OH and titanium alkoxyde $Ti[OCH(CH_3)_2]_4$ were obtained from Sigma Aldrich and were of analytical grade. The uranium metal was obtained from CETAMA, France. However, it was used and the form uranium (IV) tetrachloride solution obtained by dissolving the metal chips in 6 M of HCl solution. The final uranium concentration is about 0.5 mol/L based on ICP-AES analyses.

Pure brannerite (UTi_2O_6) was obtained in the application of the method developed by Mesbah et al.[45]. It was inspired from the synthesis protocol proposed by Martinez et al.[46] for the synthesis of uranium dioxide. The synthesis consisted in mixing U stock solution ($n_U = 2.33$ mmol) and Ti-alkoxyde ($n_{Ti} = 4.66$ mmol + 3% molar excess) in 17 mL of deionized water. Then, an excess of NH_4OH (46.6 mmol) leading to the formation of a brownish gel. The formed precursor was stirred for 30 min then washed twice in water and once in ethanol. The final recovered powder poured in 100 ml of ethanol and dried under vacuum at 40 °C leading to a final precursor with a specific surface area higher than 200 m^2/g. The obtained sample was compacted into a green pellet, and placed in a furnace for 72 h at 1300 °C under Argon continuous stream.

Solid characterization

The obtained pellets, were mechanically milled using a ball jar at 30 Hz during 30 min. The specific surface area (S_{BET}) of the ground brannerite pellets was determined using a MJ Micromeritics ASAP 2020 apparatus (BET method) under krypton at 77 K. The sample was previously heated at 333 K for 24 h. The measurement was performed three times and the obtained values ranged from 0.1 to 0.3 m^2/g.

The synthesized powder and insoluble residues of brannerite collected at the end of some of the leaching experiments were analyzed by Powder X-Ray Diffraction (PXRD) over the use of the Bruker D8 advance diffractometer (Cu $K\alpha_{1,2}$, $\lambda = 1.54184$ Å). Special sample holders (dome) were used in order to avoid any radioactive contamination. Data were collected in an angular range comprised between 5 and 100° (2θ) with steps of 0.019 for a counting time of 3 h per pattern. The crystal structure of the synthetic brannerite was refined by applying the Rietveld method using the Fullprof_package[47]. The obtained data confirmed the preparation of pure brannerite sample with $a = 9.8126(2)$ Å, $b = 3.7688(1)$ Å, $c = 6.9243(1)$ Å, $\beta = 118.94(1)°$, $V = 224.10(1)$ Å^3. Observed, calculated and the difference patterns after the crystal structure refinement is viewed in Fig. 8 (left panel). Moreover, the morphology of the brannerite sample used for the dissolution experiments was observed by scanning electron microscopy (SEM, Quanta 200, ESEM-FEG, FEI Company). The collected image presented in Fig. 8 (right panel), showed the presence of relative large grains of about 5–10 µm and of smaller debris of about 1 µm. Despite the presence of these smaller particles, the specific surface area of the sample measured by krypton adsorption and the BET method was low (i.e. between 0.3 and 0.1 m^2/g). These values of specific surface area corresponded to the geometric surface area of brannerite spheres of 3–9 µm in diameter, respectively, which indicated that the great majority of the brannerite grains were in this range of size.

Dissolution experiments

Samples of synthetic brannerite were dissolved to conduct a multi-parametric study. 25 or 50 mg of powdered brannerite were put in contact with 25 or 50 mL H_2SO_4 solution, with concentrations ranging from 0.1 to 2 mol/L in polytetrafluoroethylene container. $Fe_2(SO_4)_3$ was heated overnight in order to evacuate water molecules, then was added to H_2SO_4 solutions to obtain an Fe(III) concentration of 2.8 g/L (i.e., 0.05 mol/L). The experimental conditions considered for all the dissolution tests are summarized in Table 3. All the containers were hermetically closed and placed in different ovens at various temperatures (25, 40, 60, and 80 °C) under agitation for the duration of the experiment.

During the dissolution experiments, solution aliquots were collected with a decreasing frequency. 800 µL of solution were sampled then centrifuged at 14,000 rpm for 2 min in order to avoid the presence of colloids in the solution. Then, 500 µL of the supernatant were collected and diluted with 4.5 mL of 1 wt. % HNO_3 solution. 300 µL of the residual solution were put into the dissolution reactor along with 500 µL of fresh dissolution medium. By this way, it can be noticed that only 3% of the solution was replaced at each uptake. These conditions avoided possible strong disturbance of the surface over volume ratio during the experiment.

The elemental concentrations of uranium and titanium in solution were measured using inductively coupled plasma-atomic emission spectroscopy (ICP-AES). ICP-AES was first calibrated with U and Ti standard solutions prepared by dilution of a certified standard solution ($C_U = C_{Ti} = 1000$ ppm) with 0.2 mol/L HNO_3 solution. Four and five emission rays of U were selected (279.394, 367.007, 385.958, and 409.014 nm) for U and (307.864, 323.452, 334.0187, 334.941, and 336.121 nm) for Ti, respectively. The elemental concentrations and associated errors were estimated as the

Table 3. Experimental conditions considered for the dissolution tests performed on synthetic brannerite.

Dissolution test number	m_0 (mg)	Solution volume (mL)	$[H_2SO_4]$ (mol/L)	T (°C)	$C_{Fe(III)}$ (g/L)
1	100	100	0.1	25	0
2	100	100	1	25	0
3	100	100	2	25	0
4	100	100	0.1	25	2.8
5	100	100	1	25	2.8
6	100	100	2	25	2.8
7	100	100	0.1	40	0
8	100	100	1	40	0
9	100	100	2	40	0
10	100	100	0.1	40	2.8
11	100	100	1	40	2.8
12	100	100	2	40	2.8
13	50	50	0.1	80	0
14	50	50	1	80	0
15	50	50	2	80	0
16	50	50	0.1	80	2.8
17	50	50	1	80	2.8
18	50	50	2	80	2.8
19	50	50	0.1	60	0
20	50	50	1	60	0
21	50	50	2	60	0
22	50	50	0.1	60	2.8
23	50	50	1	60	2.8
24	50	50	2	60	2.8

average value and twice the standard deviation value of the 3 replicates of all emission lines, respectively.

Once the concentrations were measured, the relative mass loss, $\frac{\Delta m}{m_0}(t)$ (expressed in wt. %) and the normalized weight loss, $N_L(i,t)$ (expressed in g/m^2) were calculated using the initial surface area of the brannerite sample in contact with the solution and the theoretical mass fraction of the elements using the following equations:

$$\frac{\Delta m}{m_0}(t) = \frac{m_i(t)}{f_i \times m_0} \tag{3}$$

$$N_L(i,t) = \frac{m_i(t)}{f_i \times S(t)} \tag{4}$$

$m_i(t)$ (g) corresponds to the mass of element i collected in the solution at time t; m_0 (g) is the initial mass of sample introduced in the system (Table 3). S (m^2) is the surface area of brannerite in contact with the solution and f_i (g/g) represents the mass ratio of element i in the studied solid.

The surface area of the sample in contact with solution is defined as:

$$S(t) = S_{SA} \times \left(m_0 - \frac{m_i(t-1)}{f_i}\right) \tag{5}$$

where S_{SA} (m^2/g) corresponds to the initial surface area mentioned above. The mass of element i dissolved during the experiment was calculated using the concentration of each element, C_i (g/L) according to:

$$m_i = C_i \times V \tag{6}$$

where V (L) is the volume of the acidic solution introduced in the reactor as mentioned in Table 3. The normalized dissolution rate, $R_L(i)$ is obtained as the time-derivative of the normalized mass loss:

$$R_L(i) = \frac{\mathrm{d}\, N_L(i)}{\mathrm{d}t} \tag{7}$$

For all the dissolution experiments, the normalized dissolution rate are determined for $0.1\text{–}1\% \le \frac{\Delta m}{m_0} \le 50\%$. This domain corresponds to a linear variation of the normalized weight losses unlike the conditions used. Finally, the congruence ratio, R was evaluated as the ratio $R_L(U)/R_L(T_i)$.

Multiparametric expression of the normalized dissolution rate

The multiparametric description of the dissolution reaction rate was proposed by Lasaga[48] based on experimental results. In this study, only the influence of the activity of the proton and of the temperature on the dissolution rate of brannerite was considered. Thus, the general form of the rate law was simplified as follows:

$$R_L(i) = k \times \exp\left(-\frac{E_A}{RT}\right) \times (H_3O^+)^n \tag{8}$$

where k (g/(m^2 d)) is the rate constant, E_A (kJ/mol) is the apparent activation energy of the overall reaction, R is the gas constant, and T is the absolute temperature. (H_3O^+) is the activity of proton, and n is the partial order of the reaction related to the proton.

The rate law parameters k, E_A and n were fitted using the entire set of R_L(U) data obtained either in the presence or in absence of Fe(III) in solution using the JMP V14 statistical software. The nonlinear regression was done using the analytic Gauss-Newton algorithm.

The pH values were calculated from the molalities of the prepared H_2SO_4 solutions with the geochemical speciation software PHREEQC[49] associated with the Thermochimie SIT V9 thermodynamic database[50,51]. In this database, the log $K°$ (298 K) associated to the protonation equilibrium $H^+ + SO_4^{2-} \leftrightarrows HSO_4^-$ and the enthalpy of reaction reach 1.98 and 22.44 kJ/mol, respectively. The molar to molal conversion was performed using the densities of 0.1 mol/L, 1 and 2 mol/L H_2SO_4 solutions at the corresponding temperature. The density of acid solutions were calculated using the expression developed by Novotny and Sohnel[52]. Then, the activity corrections were performed using the Specific Interaction Theory (SIT) as implemented in PHREEQC. The proton activities of the various solutions calculated using PHREEQC software are summarized in Supplementary Table S1.

DATA AVAILABILITY

The datasets generated during and/or analyzed during the current study are available from the corresponding author on reasonable request.

Received: 27 January 2021; Accepted: 16 April 2021;
Published online: 02 June 2021

REFERENCES

1. Bhargava, S. K. et al. A review of acid leaching of uraninite. *Hydrometallurgy* **151**, 10–24 (2015).
2. Grandstaff, D. E. Kinetic study of dissolution of uraninite. *Economic Geol.* **71**, 1493–1506 (1976).
3. Ram, R. et al. An investigation on the dissolution of natural uraninite ores. *Miner. Eng.* **50-51**, 83–92 (2013).
4. IAEA. Uranium extraction technology. *Technical Reports Series* **359** (1993).
5. Wilde, A. et al. Geology and mineralogy of uranium deposits from Mount Isa, Australia: implications for albitite uranium deposit models. *Minerals* **3**, 258–283 (2013).
6. Pownceby, M. I. & Johnson, C. Geometallurgy of Australian uranium deposits. *Ore Geol. Rev.* **56**, 25–44 (2014).
7. Larocque, E. & Pakkala, E. Current leaching and product recovrey practice at denison-mines-limited. *Cim. Bull.* **72**, 172–176 (1979).
8. Hester, K. D. Current developments at Rio-Algom, Elliot-Lake. *Cim. Bull.* **72**, 181–188 (1979).
9. Gilligan, R. & Nikoloski, A. N. The extraction of uranium from brannerite—a literature review. *Miner. Eng.* **71**, 34–48 (2015).
10. Lottering, M. J., Lorenzen, L., Phala, N. S., Smit, J. T. & Schalkwyk, G. A. C. Mineralogy and uranium leaching response of low grade South African ores. *Miner. Eng.* **21**, 16–22 (2008).
11. Charalambous, F. A., Ram, R., Pownceby, M. I., Tardio, J. & Bhargava, S. K. Chemical and microstructural characterisation studies on natural and heat treated brannerite samples. *Miner. Eng.* **39**, 276–288 (2012).
12. Zhang, Y. et al. Recrystallisation of amorphous natural brannerite through annealing: The effect of radiation damage on the chemical durability of brannerite. *J. Nucl. Mater.* **350**, 293–300 (2006).
13. James, M. & Watson, J. N. The synthesis and crystal structure of doped uranium brannerite phases $U_{1-x}M_xTi_2O_6$ (M=Ca^{2+}, La^{3+}, and Gd^{3+}). *J. Solid State Chem.* **165**, 261–265 (2002).

14. Bowell, R. J. et al. Geometallurgy of uranium deposits. *Miner. Eng.* **24**, 1305–1313 (2011).
15. Lumpkin, G. R., Leung, S. H. F. & Ferenczy, J. Chemistry, microstructure, and alpha decay damage of natural brannerite. *Chem. Geol.* **291**, 55–68 (2012).
16. Turuani, M. et al. Geochemical fingerprints of brannerite (UTi_2O_6): an integrated study. *Mineralogical Mag.* **84**, 313–334 (2020).
17. Charalambous, F. A. *Synthesis, Characterisation and Dissolution of Brannerite. A Uranium Titanate Mineral* (RMIT University, 2013).
18. Charalambous, F. A. et al. Leaching behaviour of natural and heat-treated brannerite-containing uranium ores in sulphate solutions with iron(III). *Miner. Eng.* **57**, 25–35 (2014).
19. Charalambous, F. A., Ram, R., McMaster, S., Tardio, J. & Bhargava, S. K. An investigation on the dissolution of synthetic brannerite (UTi_2O_6). *Hydrometallurgy* **139**, 1–8 (2013).
20. Gilligan, R. & Nikoloski, A. N. Leaching of brannerite in the ferric sulphate system —Part 1: kinetics and reaction mechanisms. *Hydrometallurgy* **156**, 71–80 (2015).
21. Gilligan, R. & Nikoloski, A. N. Leaching of brannerite in the ferric sulphate system. Part 3: the influence of reactive gangue minerals. *Hydrometallurgy* **164**, 343–354 (2016).
22. Gilligan, R. & Nikoloski, A. N. Alkaline leaching of brannerite. Part 2: leaching of a high-carbonate refractory uranium ore. *Hydrometallurgy* **173**, 224–231 (2017).
23. Gilligan, R. & Nikoloski, A. N. Alkaline leaching of brannerite. Part 1: kinetics, reaction mechanisms and mineralogical transformations. *Hydrometallurgy* **169**, 399–410 (2017).
24. Gilligan, R. & Nikoloski, A. N. Leaching of brannerite in the ferric chloride system. *Hydrometallurgy* **180**, 104–112 (2018).
25. Gogoleva, E. M. The leaching kinetics of brannerite ore in sulfate solutions with iron(III). *J. Radioanalytical Nucl. Chem.* **293**, 185–191 (2012).
26. Hussein, A., Tardio, J. & Bhargava, S. in *CHEMECA 2008* (Engineers Australia).
27. Ring, R. J. Ferric sulphate leaching of some australian uranium ores. *Hydrometallurgy* **6**, 89–101 (1980).
28. Zhang, Y. et al. Dissolution of synthetic brannerite in acidic and alkaline fluids. *J. Nucl. Mater.* **321**, 1–7 (2003).
29. Costine, A., Nikoloski, A. N., Da Costa, M., Chong, K. F. & Hackl, R. Uranium extraction from a pure natural brannerite mineral by acidic ferric sulphate leaching. *Miner. Eng.* **53**, 84–90 (2013).
30. Yudintsev, S. V., Stefanovsky, S. V., Nikol'skii, M. S., Stefanovskaya, O. I. & Nikonov, B. S. Brannerite, UTi_2O_6: Crystal chemistry, synthesis, properties, and use for actinide waste immobilization. *Radiochemistry* **58**, 333–348 (2016).
31. Stefanovsky, S. V., Yudintsev, S. V., Shiryaev, A. A., Murzin, V. Y. & Trigub, A. L. Phase partitioning and uranium speciation in brannerite-based ceramics. *J. Eur. Ceram. Soc.* **37**, 771–777 (2017).
32. Zhang, Y. et al. Kinetics of uranium release from Synroc phases. *J. Nucl. Mater.* **289**, 254–262 (2001).
33. Zhang, Y. J. et al. Development of brannerite glass-ceramics for the immobilization of actinide-rich radioactive wastes. *J. Am. Ceram. Soc.* **100**, 4341–4351 (2017).
34. Thomas, B. S. & Zhang, Y. A kinetic model of the oxidative dissolution of brannerite, UTi_2O_6. *Radiochimica Acta* **91**, 463–472 (2003).
35. Cordara, T. et al. Kinetics of dissolution of UO_2 in nitric acid solutions: a multiparametric study of the non-catalysed reaction. *J. Nucl. Mater.* **496**, 251–264 (2017).
36. Shoesmith, D. W. Fuel corrosion processes under waste disposal conditions. *J. Nucl. Mater.* **282**, 1–31 (2000).
37. Shoesmith, D. W., Kolar, M. & King, F. A mixed-potential model to predict fuel (uranium dioxide) corrosion within a failed nuclear waste container. *Corrosion* **59**, 802–816 (2003).
38. Shoesmith, D. W., Sunder, S. & Tait, J. C. Validation of an electrochemical model for the oxidative dissolution of used CANDU fuel. *J. Nucl. Mater.* **257**, 89–98 (1998).
39. Sunder, S., Shoesmith, D. W. & Miller, N. H. Oxidation and dissolution of nuclear fuel (UO2) by the products of the alpha radiolysis of water. *J. Nucl. Mater.* **244**, 66–74 (1997).
40. King, F., Kolar, M. & Shoesmith, D. W. in *Scientific Basis for Nuclear Waste Management Xxii*, (eds D. J. Wronkiewicz & J. H. Lee) Vol. 556, *Materials Research Society Symposium Proceedings* 463–470 (1999).
41. Carbol, P., Wegen, D. H., Wiss, T. & Fors, P. in *Comprehensive Nuclear Materials* (ed Rudy J. M. Konings) 389–420 (Elsevier, 2012).
42. Sunder, S., Shoesmith, D. W. & Miller, N. H. in Scientific Basis for Nuclear Waste Management Xviii, Pts 1 and 2, (eds T. Murakami & R. C. Ewing) Vol. 353, *Materials Research Society Symposium Proceedings* 617-624 (1995).
43. Guillaumont, R. et al. Update on the Chemical Thermodynamics of Uranium, Neptunium, Plutonium, Americium and Technetium. *Chemical Thermodynamics, 5, OECD-NEA Eds* (2003).
44. Lasaga, A. C. & Kirkpatrick, R. J. *Kinetics of geochemical processes*, Vol. 8 (Mineralogical Society of America, 1981).
45. Mesbah, A. et al. Direct synthesis of pure brannerite UTi_2O_6. *J. Nucl. Mater.* **515**, 401–406 (2019).
46. Martinez, J. et al. An original precipitation route toward the preparation and the sintering of highly reactive uranium cerium dioxide powders. *J. Nucl. Mater.* **462**, 173–181 (2015).
47. Roisnel, T. & Rodríguez-Carvajal, J. in Materials Science Forum Vol. 378–381 118–123 (2001).
48. Lasaga, A. C. in *Chemical Weathering Rates of Silicate Minerals* Vol. 31 *Reviews in Mineralogy* (eds A. F. White & S. L. Brantley) 23–86 (1995).
49. Parkhurst, D. H. & Appelo, C. A. J. *User's Guide to PHREEQC (Version 2)—A Computer Program for Speciation, Batch-Reaction, One-Dimensional Transport, and Inverse Geochemical Calculations*. (U.S.G.S Water-Resources Investigations Report 99-4259, 1999).
50. Giffaut, E. et al. Andra thermodynamic database for performance assessment: ThermoChimie. *Appl. Geochem.* **49**, 225–236 (2014).
51. Grivé, M., Duro, L., Colàs, E. & Giffaut, E. Thermodynamic data selection applied to radionuclides and chemotoxic elements: an overview of the ThermoChimie-TDB. *Appl. Geochem.* **55**, 85–94 (2015).
52. Novotny, P. & Sohnel, O. Densities of binary aqueous solutions of 306 inorganic substances. *J. Chem. Eng. Data* **33**, 49–55 (1988).

ACKNOWLEDGEMENTS

The present work was supported by the UTiLE project funded by French NEEDS Ressources program (CNRS/CEA/ORANO). The authors are gratefull to Damien Perret (CEA) for his valuable help regarding the fit of the multiparametric expression of the dissolution rate.

AUTHOR CONTRIBUTIONS

H.L, S.S., and A.M: conducted the experiments, analyzed the results, plotted the figures, and wrote the first draft, AM. S.S., and N.D. designed the experiments, wrote and finalized the manuscript. All the co-authors mounted the UTiLE/NEEDS program, contributed to the overall project, designed the experiments, and contributed to the draft and the final version of the manuscript.

COMPETING INTERESTS

The authors declare no competing interests.

ADDITIONAL INFORMATION

Supplementary information The online version contains supplementary material available at https://doi.org/10.1038/s41529-021-00173-6.

Correspondence and requests for materials should be addressed to S.S. or A.M.

Reprints and permission information is available at http://www.nature.com/reprints

Publisher's note Springer Nature remains neutral with regard to jurisdictional claims in published maps and institutional affiliations.